ELSEVIER

Journal of Organometallic Chemistry 557 (1998) 163–167

Journal of Organometallic Chemistry

Hydride abstraction from $[PPN]_2[HSb\{Fe(CO)_4\}_3]$ by alkyl iodides Synthesis and characterization of $[PPN][Sb(Me)I\{Fe(CO)_4\}_2]$

Jaap Willem van Hal, Joseph L. Stark, Kenton H. Whitmire *

Department of Chemistry, MS 60, Rice University, 6100 Main Street, Houston TX 77005-1892, USA

Received 23 April 1997; received in revised form 23 September 1997

Abstract

$[PPN]_2[HSb\{Fe(CO)_4\}_3]$ ($[PPN]_2$[**I**]) was reacted with MeI and EtI. The reaction with MeI yielded $[PPN][Sb(Me)I\{Fe(CO)_4\}_2]$ ([PPN][**II**]) whereas the reaction with EtI yielded $[PPN]_2[ISb\{Fe(CO)_4\}_3]$ ($[PPN]_2$[**III**]) instead. The structure of [PPN][**II**] was determined by single crystal X-ray diffraction. [PPN][**II**] crystallizes in the monoclinic space group $C2/c$ ($\#$ 15) with $a = 14.115(3)$ Å, $b = 17.123(3)$ Å, $c = 18.913(4)$ Å, $\beta = 97.06(3)$, $V = 4536.4(16)$ Å^3, $Z = 4$, R_1 ($I > 2\sigma(I)$) = 0.0691 and $wR_2 = 0.1900$. Analysis of the off gases indicated the presence of methane for [PPN][**II**] and ethane for $[PPN]_2$[**III**]. The possibility of the formation of $[PPN]_2$[**III**] via a radical chain mechanism was excluded by performing the reaction at high dilution, in the dark and in the presence of BHT.

Keywords: X-ray diffraction; Radical chain mechanism; Carbonyl compounds

1. Introduction

The presence of a lone pair on the main group metal fragment incorporated in transition metal carbonyl compounds has profound effects on the reactivity, stability and structural arrangement. For instance, $[HAs\{Fe(CO)_4\}_3]^{2-}$ forms $[As_2Fe_5(CO)_{17}]^{2-}$ when subjected to pyrolysis or photolysis [1] while the isoelectronic compounds $[E\{Fe(CO)_4\}_3]^{2-}$ (E = Se, Te) or $Bi\{Co(CO)_4\}_3$ simply close to form $[EFe_3(CO)_9]^{2-}$ and $BiCo_3(CO)_9$, respectively [2,3]. Because of this influence on the reactivity, we treated $[HSb\{Fe(CO)_4\}_3]^{2-}$ with alkyl halides. Previous work on the $[Sb\{Fe(CO)_4\}_4]^{3-}$ and $[RSb\{Fe(CO)_4\}_3]^{2-}$ ions showed that alkylation at the Sb atom occurs [4].

2. Experimental section

2.1. General methods

Unless otherwise specified, all synthetic manipulations were performed on a Schlenk line or in a dry box under a atmosphere of purified nitrogen using standard inert atmosphere techniques [5]. All solvents were distilled under nitrogen from the appropriate drying agents [6,7]. Solution infrared spectra were obtained in 0.1 mm CaF_2 cells by using a Perkin–Elmer 1640 Fourier Transform infrared spectrometer. ^1H and ^{13}C spectra were recorded on a Bruker AC-250 spectrometer, operating at 250 MHz for ^1H and 62.9 MHz for ^{13}C. ESI mass spectra were obtained on a Finnigan MAT 90 in MeOH in the negative ion mode. EI Mass spectroscopy was performed on a Finnigan 3300 spectrometer. Elemental analysis (C, H, N, I) was performed by National Chemical Consulting, Tenafly, NJ. EDAX (Energy Dispersive Analytical X-ray Spec-

* Corresponding author.

0022-328X/98/$19.00
PII S0022-328X(97)00681-5

troscopy) was obtained using a Cameca SX-50 microprobe with a SUN based control and data reduction system. $[PPN]_2[HSb\{Fe(CO)_4\}_3]$ ($[PPN]_2$[**I**]) was prepared by the literature method [8].

2.2. Synthesis of [PPN][Sb(I)Me{Fe(CO)$_4$}$_2$], [PPN][II]

Excess MeI (1.0 ml) was added to a solution of 1.0 g of $[PPN]_2$[**I**] in THF. After stirring overnight, the solution was filtered to remove a small amount of white precipitate and the solvent was removed in vacuo. The residue was extracted with two portions of ether (40 ml) and the extracts were concentrated. The product crystallized as red plates upon standing at room temperature in 150 mg yield (0.13 mmol; 22%). IR (ν_{CO}, cm^{-1}, CH_2Cl_2): 2038, 2016, 1924. NMR (δ, ppm, d_3-MeCN):^{1}H: 7.90–7.24 $(PPN)^+$, 2.92 CH_3; ^{13}C 216.4 (CO); 134.7–127.5 $(PPN)^+$, 12.5 CH_3. ESI (598, M^-). Elemental analysis, % calc (% found):% C 47.49 (47.44); % H 2.92 (2.82); % N 1.23 (1.49), % I 11.15 (12). The residue from the ether extraction contains I and Fe, but no Sb (by EDS).

2.3. Synthesis of [PPN]$_2$[ISb{Fe(CO)$_4$}$_3$], [PPN]$_2$[III]

This reaction was performed as described above but EtI was used instead of MeI. Upon standing at RT overnight, the product was isolated as a purple crystalline material in 0.80 g yield (0.44 mmol; 75%). IR (ν_{CO}, cm^{-1}, THF) 2024, 1991, 1925, 1907. NMR (δ ppm, d_3-MeCN):^{1}H: 7.65–7.45 $(PPN)^+$; ^{13}C 219.50 (CO), 135–127.7 $(PPN)^+$. Elemental analysis, % calc (% found): % C 55.15 (55.11); H 3.31 (3.77); N 1.53 (1.54), I 6.94 (6.50). An X-ray structure analysis of $[PPN]_2$[**III**] was attempted but severe crystallographic problems prevented a complete analysis. Two lattice choices were possible: a primitive hexagonal cell ($a = b = 24.133$ Å, $c = 13.123$ Å) and a monoclinic C-centered setting ($a = 41.793$ Å, $b = 24.125$ Å, $c = 13.123$ Å, $\beta = 90.04°$). The structure could not be solved at all in the lower monoclinic setting, but in the hexagonal setting, a cluster anion $[ISb\{Fe(CO)_4\}_3]^{2-}$ could be clearly seen and refined reasonably. However, the rest of the structure did not resolve and the refinement of the structure was therefore abandoned.

2.4. Conversion of [PPN]$_2$[ISb{Fe(CO)$_4$}$_3$], [PPN]$_2$[III] to [PPN][Sb(I)Me{Fe(CO)$_4$}$_2$], [PPN][II]

$[PPN]_2$[**III**] (0.25 g) was dissolved in THF and excess MeI (0.20 ml) was added. The solution was stirred overnight leading to the formation of a dark red solution and a small amount of white precipitate. The solution was filtered through celite and volatiles were removed by vacuum. The residue was extracted into ether, concentrated and allowed to stand at room temperature leading to the formation of crystalline material. (0.12 g, 70% yield based on Sb). The spectroscopic properties match those of samples obtained by the direct route.

2.5. Analysis of the off gases

The off gases formed during the synthesis of [PPN][**II**] and $[PPN]_2$[**III**] were analyzed using the following procedure. A pressure flask was charged with $[PPN]_2$[**I**] and evacuated on the vacuum line. THF, which had been degassed by three successive freeze, pump, thaw, degas cycles was distilled bulb to bulb on top of the solid, after which MeI or EtI was distilled on top of the frozen THF. The flask was closed, warmed to RT and the solution was stirred overnight. The off gasses of the reaction $[PPN]_2$[**I**] with MeI forming [PPN][**II**] were collected at -196°C while those of the reaction EtI with $[PPN]_2$[**I**] forming $[PPN]_2$[**III**] were collected at -78°C. The E.I. mass spectrum of the gasses indicated the presence of methane for [PPN][**II**] and the presence of HI and ethane for $[PPN]_2$[**III**]. Owing to the vapor pressure of THF at -78°C, the off gases could not be quantified.

2.6. X-ray crystallography

All crystals selected for data collection were mounted on the tip of a glass fiber with epoxy resin. Data were collected at -50°C on a Rigaku AFC5-S automated four circle diffractometer using the TEXSAN 5.0 soft-

Table 1
Crystal data for [PPN][**II**]

Empirical formula	$C_{45}H_{33}Fe_2INO_8P_2Sb$
Formula weight (g/mol)	1138.01
Crystal System	Monoclinic
Space group	C 2/c (# 15)
a (Å)	14.115(3)
b (Å)	17.123(3)
c (Å)	18.913(4)
β (°)	97.06(3)
Volume (Å^3)	4536.4(16)
Z	4
ρ (calc.), Mg/m^3	1.666
Temperature (K)	223
μ (Mo–K$_\alpha$), mm^{-1}	2.025
GOF on F^2	1.067
R_1 [$I > 2\sigma(I)$]	0.0691
wR^2 [$I > 2\sigma(I)$]	0.1900
Tranmission range	0.9–1.0
Reflections collected	6600
Independent reflections	3305 [$R_{int} = 0.0198$]
F(000)	2240
Radiation: λ, Å	MoK$_\alpha$;0.7107
Color	Red

$R_1 = \Sigma||F_o| - |F_c||/-|F_o|$. $wR^2 = [\Sigma w(F_o^2 - F_c^2)^2]/\Sigma[w(F_o^2)^2]]^{0.5}$.
$w = [\sigma^2(Fo^2) + (aP)^2 + bP]^{-1}$ where $P = (F_o^2 + 2F_c^2)/3$.

Table 2
Atomic coordinates and equivalent isotropic displacement parameters (Å^2) for [PPN][**II**]

Atom	x	y	z	$U_{(eq)}$	Occupancy
Sb(1)	0.0000	0.53469(5)	0.2500	0.0490(4)	1
Fe(1)	0.01240(8)	0.60547(7)	0.13542(6)	0.0328(4)	1
I(1)	0.1071(2)	0.41328(13)	0.26274(10)	0.1027(8)	0.50
C(1)	0.1071(2)	0.41328(13)	0.26274(10)	0.1027(8)	0.50
C(11)	0.0234(7)	0.6608(6)	0.0585(5)	0.044(2)	1
C(12)	−0.0708(8)	0.6739(7)	0.1633(5)	0.055(3)	1
C(13)	−0.0320(7)	0.5206(7)	0.0891(5)	0.051(3)	1
C(14)	0.1369(8)	0.6070(6)	0.1619(6)	0.053(3)	1
O(11)	0.0305(6)	0.6981(5)	0.0092(4)	0.072(2)	1
O(12)	−0.1243(8)	0.7186(6)	0.1801(5)	0.093(3)	1
O(13)	−0.0577(8)	0.4651(6)	0.0584(5)	0.095(4)	1
O(14)	0.2179(6)	0.6075(5)	0.1774(6)	0.087(3)	1
N(1)	0.0000	0.9157(6)	0.2500	0.036(2)	1
P(1)	0.00502(14)	0.94307(12)	0.17109(10)	0.0270(5)	1
C(111)	−0.0979(6)	0.9093(5)	0.1140(4)	0.030(2)	1
C(112)	−0.1875(7)	0.9170(7)	0.1354(5)	0.051(3)	1
C(113)	−0.2668(7)	0.8945(8)	0.0913(6)	0.067(3)	1
C(114)	−0.2599(8)	0.8641(7)	0.0257(6)	0.059(3)	1
C(115)	−0.1709(7)	0.8541(7)	0.0038(5)	0.053(3)	1
C(116)	−0.0912(7)	0.8774(6)	0.0470(4)	0.041(2)	1
C(121)	0.0130(6)	1.0464(5)	0.1595(4)	0.032(2)	1
C(122)	0.0906(6)	1.0864(5)	0.1947(4)	0.039(2)	1
C(123)	0.0973(8)	1.1677(6)	0.1881(5)	0.050(2)	1
C(124)	0.0271(8)	1.2083(6)	0.1477(5)	0.053(3)	1
C(125)	−0.0503(8)	1.1695(6)	0.1124(5)	0.049(2)	1
C(126)	−0.0578(6)	1.0887(5)	0.1187(4)	0.038(2)	1
C(131)	0.1075(6)	0.9037(5)	0.1368(4)	0.031(2)	1
C(132)	0.1461(6)	0.8326(5)	0.1628(5)	0.043(2)	1
C(133)	0.2218(7)	0.8007(6)	0.1313(7)	0.058(3)	1
C(134)	0.2581(7)	0.8375(6)	0.0762(6)	0.052(3)	1
C(135)	0.2206(7)	0.9075(6)	0.0515(5)	0.048(2)	1
C(136)	0.1453(6)	0.9407(5)	0.0814(4)	0.039(2)	1

$U_{(eq)}$ is defined as one third of the trace of the orthogonalized U_{ij} tensor.

ware package, and were corrected for Lorentz/polarization effects [9]. The data of [PPN]$_2$[**II**] was corrected for absorption using Ψ-scans. Data collection and refinement parameters are summarized in Table 1. Scattering factors were taken from the literature. The structure was solved using the SHELXTL-PLUS package on a PC [10]. Refinements on F^2 using all reflections except those with very negative F^2 were performed with SHELXL-93 on a PC or a SUN workstation running SOLARIS [11]. Weighted R-factors (wR) and all goodnesses of fit (S) are based on F^2, conventional R-factors (R) are based on F, with F set to zero for negative F^2. R-factors based on F^2 are statistically about twice as large as those based on F. The weighting factor $w = [\sigma^2(F_o^2) + (aP)^2 + bP]^{-1}$ where $P = (F_o^2 + 2F_c^2)/3$ was refined for a and b. Hydrogen atoms were included in their calculated positions (Table 2).

The structure of [PPN][**II**] can be refined in either a triclinic or monoclinic setting. In either setting, the initial solution showed a maximum in electron density at 2.5 Å from the Sb atom. This was determined to represent a statistical disorder between the I and Me positions. The structure was refined in the monoclinic setting with a virtual atom of equal components I and C (Table 3).

3. Results and discussion

The reaction of MeI with [PPN]$_2$[**I**] forms [PPN][**II**] (Fig. 1) in reasonable yield. The net result is that MeI has oxidatively added to the Sb center. Analysis of the off gases of this reaction indicated the presence of methane gas. The remaining residue after the extraction with Et_2O contains no Sb but does still contain Fe, P and CO (EDAX/IR). The residue dissolved in THF but the IR spectrum in the ν_{CO} region was weak and the pattern did not match any of the known iron carbonyl hydrides. This is consistent with the reaction of [**I**]$^{2-}$ with MeI to first form methane and the [**III**]$^{2-}$ ion (Scheme 1) which then subsequently reacts with a second equivalent of MeI. The reaction of [PPN]$_2$[**III**] with MeI in THF does indeed form [PPN][**II**], thus confirming this hypothesis. Although the interpretation of the

Table 3
Selected bond distances (Å) and angles (°)

Sb(1)–Fe(1)#1	2.5078(13)	Sb(1)–Fe(1)	2.5078(13)
Sb(1)–X#1	2.564(2)	Sb(1)–X	2.564(2)
Fe–C range	1.758(9)–1.784(12)		
C–O range	1.145(11)–1.149(12)		
Fe(1)#1–Sb(1)–Fe(1)	122.20(7)	Fe(1)#1–Sb(1)–X#1	111.72(6)
Fe(1)–Sb(1)–X#1	114.43(6)	Fe(1)#1–Sb(1)–X	114.43(6)
Fe(1)–Sb(1)–X	111.72(6)	X#1–Sb(1)–X	71.66(12)
Fe–C–O range	177.7(10)–178.8(9)		

Symmetry transformations used to generate equivalent atoms: #1 $-x, y, -z+1/2$.
X denotes the virtual atoms composed of equal components I and C

bond metricals is severely handicapped by the statistical disorder between C and I, the identity of the product is certain. The negative ion ESI mass spectrum shows clearly the parent ion $[\mathbf{II}]^-$. All other spectroscopic properties are also in agreement with the structure. The unit cell constants of several crystals of two batches were all identical. In addition to the spectroscopic data, EDAX showed no significant amounts of Cl in either the crystals or the starting material. The absence of Cl had to be confirmed since the average electron density between C and I also corresponds reasonably well to that of a Cl atom. The Cl could have been introduced to $[\mathbf{I}]^{2-}$ upon the addition of [PPN]Cl. The disorder in the I/Me bond is probably caused by the semi-twofold symmetry of the Sb–Fe bond as well as the PPN^+ cation. Refinement in the lower triclinic setting did not solve the disorder problem. Therefore, the structure was refined in the monoclinic C-centered setting.

These results contrast with earlier alkylation studies using the $[Sb\{Fe(CO)_4\}_4]^{3-}$ and the $[RSb\{Fe(CO)_4\}_3]^{2-}$ anions, for which alkylation at the Sb atom was observed [4]. The presence of a lone pair on the main group metal fragment incorporated in transition metal carbonyl compounds has profound effects on the reactivity, stability and structural arrangement. For instance, $[HAs\{Fe(CO)_4\}_3]^{2-}$ forms $[As_2Fe_5(CO)_{17}]^{2-}$ when subjected to pyrolysis or photolysis [1], while the isoelectronic compounds $[E\{Fe(CO)_4\}_3]^{2-}$ (E = Se, Te) or $Bi\{Co(CO)_4\}_3$ simply close to form $[EFe_3(CO)_9]^{2-}$ and $BiCo_3(CO)_9$ respectively [2,3].

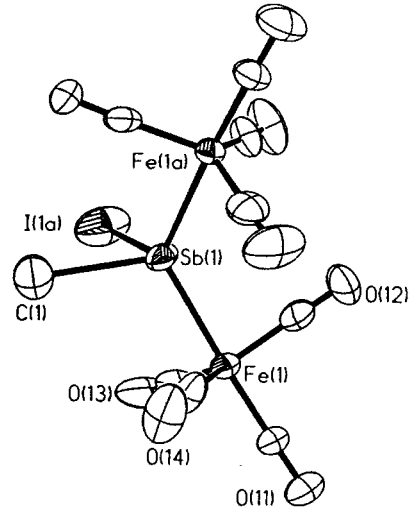

Fig. 1. Thermal ellipsoid plot of $[\mathbf{II}]^-$ (50% probability).

In order to overcome this disorder problem and to gain insight into the reaction mechanism, the alkylation reaction was also performed with EtI; however, the reaction of EtI with $[PPN]_2[\mathbf{I}]$ yielded $[PPN]_2[\mathbf{III}]$ cleanly and in good yield. Severe disorder problems prevented full crystallographic characterization of $[PPN]_2[\mathbf{III}]$. However, on the basis of comparison of the spectroscopic data with the known $[ClSb\{Fe(CO)_4\}_3]^{2-}$ and analyses, the identity of $[PPN]_2[\mathbf{III}]$ is clear [12,13]. A possible mechanism for the formation of $[\mathbf{III}]^{2-}$ is a radical dehalogenation in Scheme 1. Another possible mechanism is a Würtz-type reduction of the carbon–halogen bond. This proceeds similarly to the radical dehalogenation chain mechanism shown above, except that both radical species do not propagate the reaction but react with each other. Similarly, this dehalogenation might also proceed via an ionic mechanism. Another possibility is the oxidative insertion of Sb into the C–I bond as depicted in Scheme 1. Analysis of the off gases showed the presence of HI and ethane, which is consistent with all three mechanisms. If this dehalogenation reaction occurs via a radical chain mechanism, it should not occur at low concentrations, in the dark or in the presence of a radical scavenger, such as BHT. However, $[\mathbf{III}]^{2-}$, can be obtained by slow diffusion of EtI into a THF solution of $[\mathbf{I}]^{2-}$. If all light is excluded $[\mathbf{III}]^{2-}$ is still formed. It is also formed in the presence of an 8-fold excess (with respect to $[\mathbf{IV}]^{2-}$) of BHT. $[\mathbf{I}]^{2-}$ itself does not react with BHT. Therefore, the radical chain mechanism can be ruled out. This once again shows how subtle changes on the main group element can change the reactivity drastically. The most likely reaction pathway is the oxidative insertion of Sb into the C–I bond, although neither a Würtz-type cou-

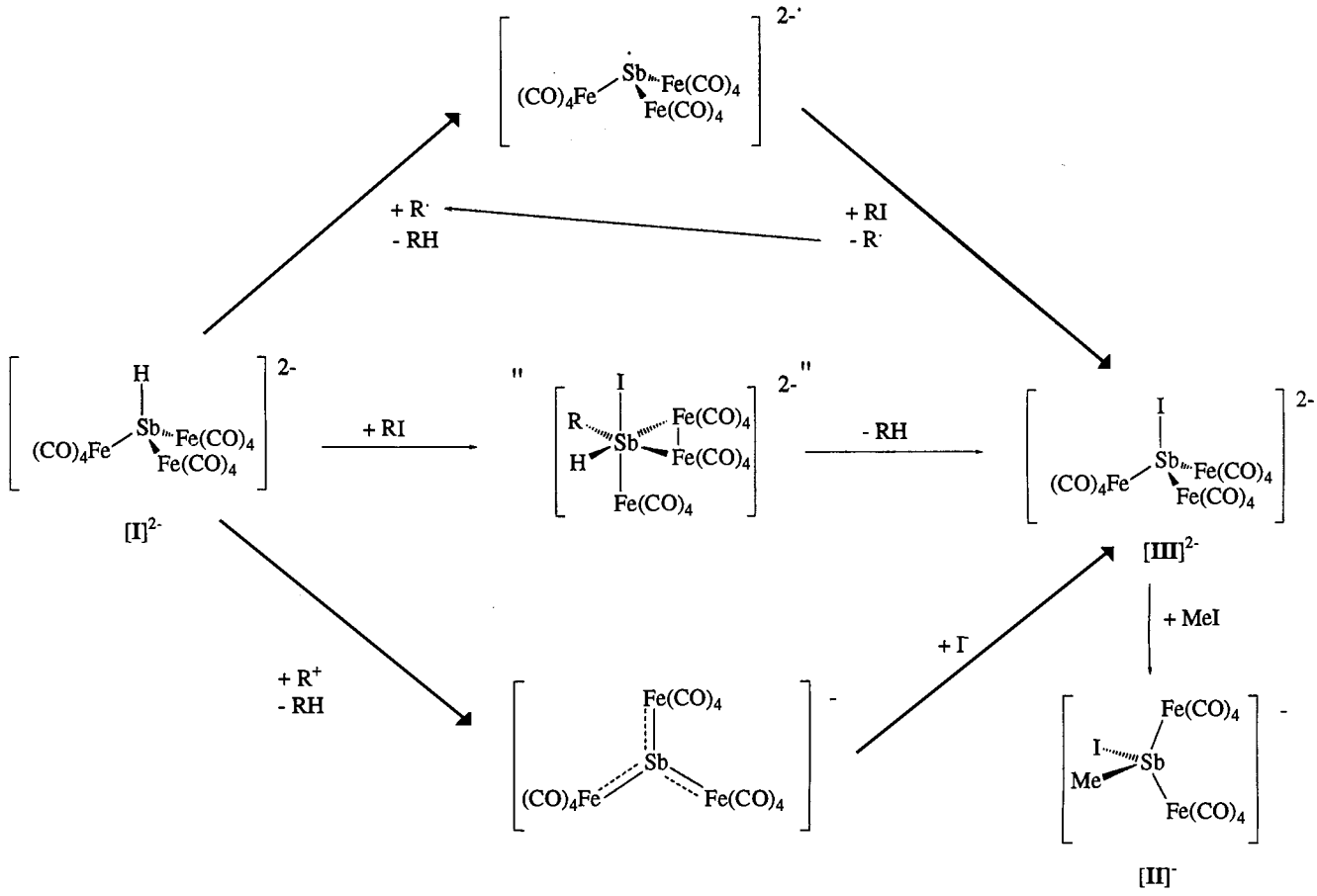

Scheme 1.

pling or a oxidative insertion process involving one of the Fe atoms can be ruled out.

4. Conclusions

The reactions of [PPN][**I**] with alkyl halides shows that the proton attached to Sb is hydridic resulting in formation of R–H. The formation of [PPN][**II**] in the case of R(Me proceeds via $[PPN]_2$[**III**], which itself forms via dehalogenation of MeI by Sb–H.

Supporting information is available on crystallographic data for $[PPN_2]$[**II**] is available in the Cambridge Crystallographic Data Base on quoting the full journal reference.

Acknowledgements

This work was assisted by a grant from the Robert A. Welch foundation and the National Science Foundation (Grant CHE-9408613). We also wish to thank Dr Terry D. Marriott for collecting mass spectrometric data.

References

[1] R.E. Bachman, K.H. Whitmire, Organometallics 14 (1995) 796.
[2] R.E. Bachman, K.H. Whitmire, Inorg. Chem. 33 (1994) 2527.
[3] K.H. Whitmire, J.S. Leigh, M.E. Gross, J. Chem. Soc. Chem. Commun. (1987) 926.
[4] M. Shieh, C.-M. Sheu, L.-L. Ho, J.-J. Cherng, L.-F. Jang, C.-H. Ueng, S -M. Peng, G.-H. Lee, Inorg. Chem. 35 (1996) 5504.
[5] D.F. Shriver, M.A. Drezdon, The Manipulation of Air Sensitive Compounds, Wiley, New York, 1986.
[6] A.J. Gordon, R.A. Ford, The Chemist's Companion, John Wiley, New York, 1972.
[7] A.B. Pangborn, M.A. Giardello, R.H. Grubbs, R. K. Rosen, F.J. Timmers, Organometallics 15 (1996) 1518.
[8] P. Henderson, M. Rossignoli, R.C. Burns, M.L. Scudder, D.C. Craig, J. Chem. Soc. Dalton Trans. (1994) 1641.
[9] TEXSAN: Single Crystal Structure Analysis Software 5.0, Molecular Structure Company, The Woodlands, TX, 1990.
[10] G.M. Sheldrick, SHELXL-93, Göttingen, Germany, 1993.
[11] G.M. Sheldrick, SHELXTL PLUS PC 5.0, Siemens Crystallographic Research Systems, Madison, WI, 1995.
[12] S. Luo, K.H. Whitmire, Inorg. Chem. 28 (1989) 1424.
[13] A.A. Trifonov, P. Van de Weghe, J. Collin, A. Domingos, I. Santos, J. Organomet. Chem. 527 (1997) 225.